Supporting Information

Layer-structured $K_{0.5}Mn_{0.8}Cu_{0.1}Mg_{0.1}O_2$ for High-performance Potassium-ion Batteries by Alleviating the Phase Transformation

Hong Chen[‡], Xuan-Wen Gao[‡], Qi Li, Run-Ze Niu, Shuai-Shuai Wang, Qin-Fen Gu, Jian-jia Mu, Wen-Bin Luo*

Institute for Energy Electrochemistry and Urban Mines Metallurgy, School of Metallurgy, Northeastern University, Liaoning, 110819, China

Corresponding Authors

E-mail: luowenbin@smm.neu.edu.cn

Experimental

Materials preparation

The KMCMO cathode material was synthesized through a sol-gel method and a solid-state reaction at high temperature. The raw materials used were potassium carbonate, manganese acetate tetrahydrate, copper acetate, and magnesium acetate tetrahydrate, with citrate acting as a cheating agent. The molar ratio of the raw materials was 0.25:0.8:0.1:0.1:12. To synthesize the KMCMO material, citric acid was dissolved in deionized water and heated. A mixed solution of Mn^{2+}, Cu^{2+}, and Mg^{2+} dissolved in water, as well as a K^+ solution dissolved in water, were added to the citric acid solution with magnetic stirring. The mixture was stirred until a wet gel formed, then dried and ground. The resulting mixture was calcined at high temperatures. The KMCMO product was cooled and transferred into an argon-filled glovebox to prevent moisture absorption. For comparison, other materials were synthesized using the same procedure but without the addition of reagents containing Cu/Mg.

Material Characterization

The crystal structure analysis was conducted utilizing a Bruker D8 Advance Diffractometer, employing a scanning rate of 5° min^{-1}. The resulting XRD patterns were refined through the utilization of GSAS software. In situ XRD analysis was also performed on the electrodes within the 2θ range of 10° to 45°, employing a scanning rate of 5° min^{-1}. The morphology and microstructure of the samples were examined using scanning electron microscopy (SEM SU8220, Hitachi High-Tech Company) and high-resolution transmission electron microscopy (HRTEM). The elemental composition of the samples was analysed through energy dispersive spectrometry (EDS), and elemental maps were generated utilizing a super-X EDS detector system (Bruker; Super-X, USA). Furthermore, the elemental chemical compositions of the materials were determined using X-ray photoelectron spectroscopy (XPS, Thermo ESCALAB 250XI Al K α X-ray source).

Electrochemical Tests

The electrodes were prepared by combining the as-synthesized material (80 wt.%), acetylene black (10 wt.%), and polytetrafluoroethylene (10 wt.%) in N-methyl-2-pyrrolidone. The resulting slurry was then cast onto an aluminium foil and dried at 120 °C under vacuum overnight. The dried film was cut into discs with a diameter of 12 mm. The electrode film, coated on the aluminium foil, was weighed and assembled into a 2032 coin-cell with a glass filter. A potassium metal foil was used as the counter/reference electrode. The cathode active mass loading was approximately 1.5-2.0 mg cm^{-2} per electrode. In the K-ion full cell assembly, a cathode-to-anode mass loading ratio of 1.2:1 was maintained. The electrolyte consisted of 0.8 M potassium hexafluorophosphate (KPF$_6$, 99.5%, Sigma-Aldrich) dissolved in a mixture of ethylene carbonate and propylene carbonate (EC/PC, 1/1). Cyclic voltammetry (CV) tests were conducted using an LANHE instrument electrochemical workstation, with scan rates specified,

within a voltage range of 1.5 to 4 V versus K^+/K. Electrochemical impedance spectroscopy (EIS) was performed using a Princeton 2273 test measurement system, with frequencies ranging from 100 KHz to 10 mHz.
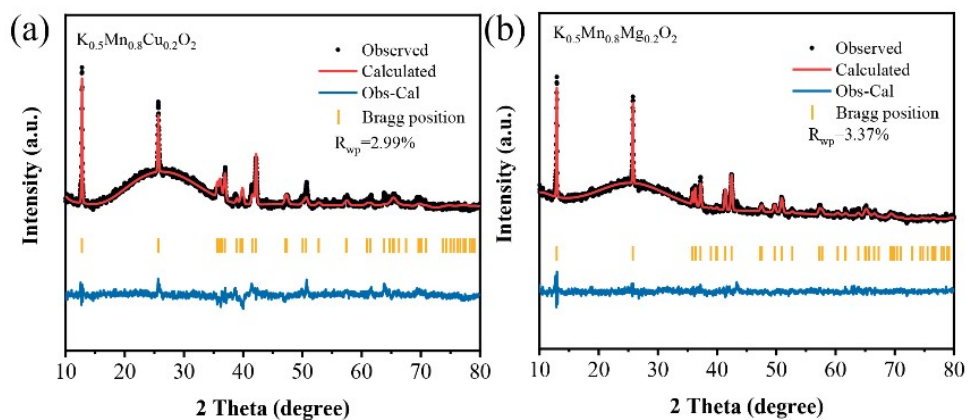

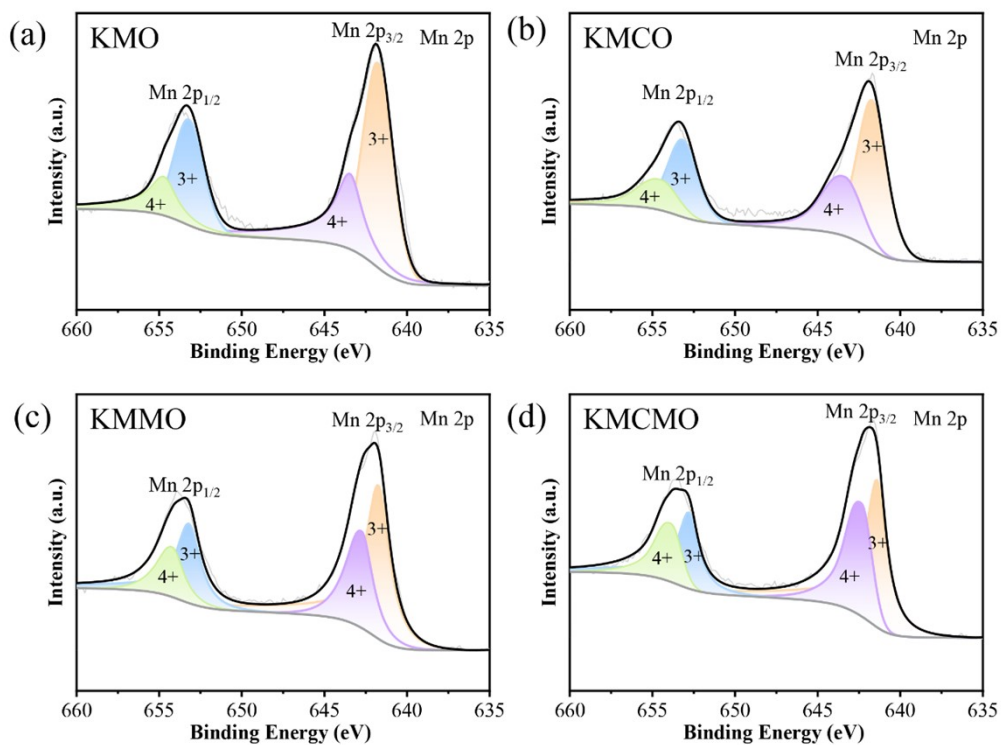**Figure S1.** Rietveld refinement results of KMMO (a) and KMCO (b)

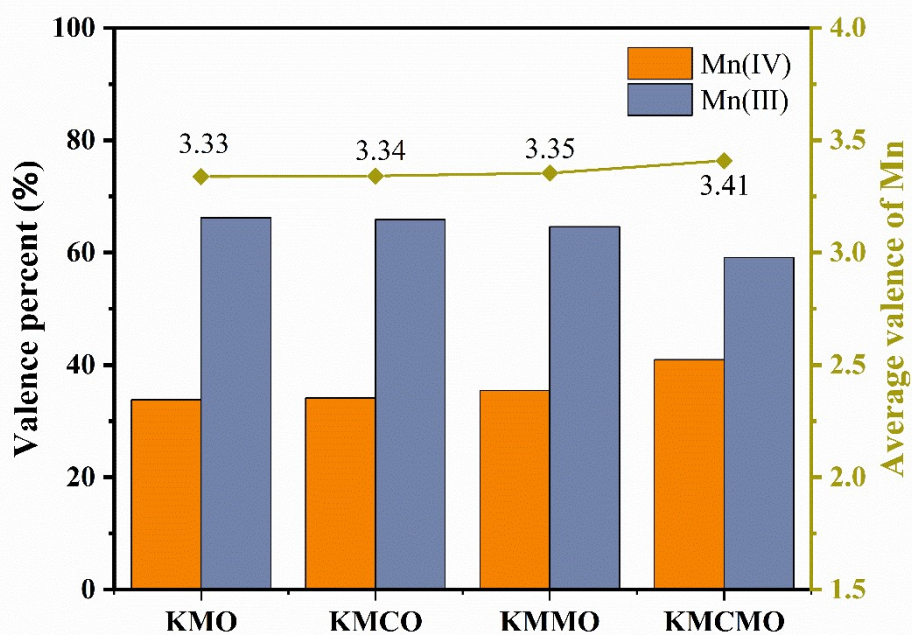**Figure S2**. Mn 2p XPS spectrum and fitting lines for a) KMO, b) KMCO, c) KMMO and d) KMCMO.

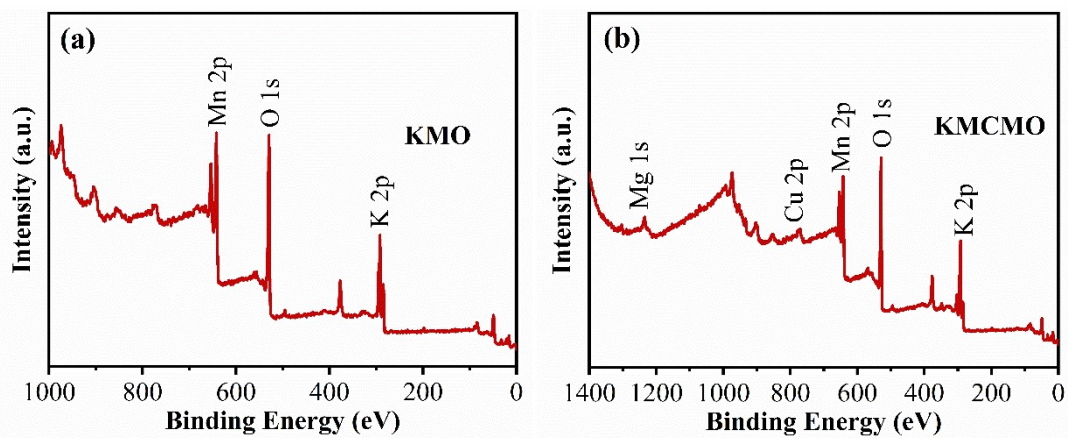**Figure S3**. Corresponding statistics of fitting results and average valences of Mn

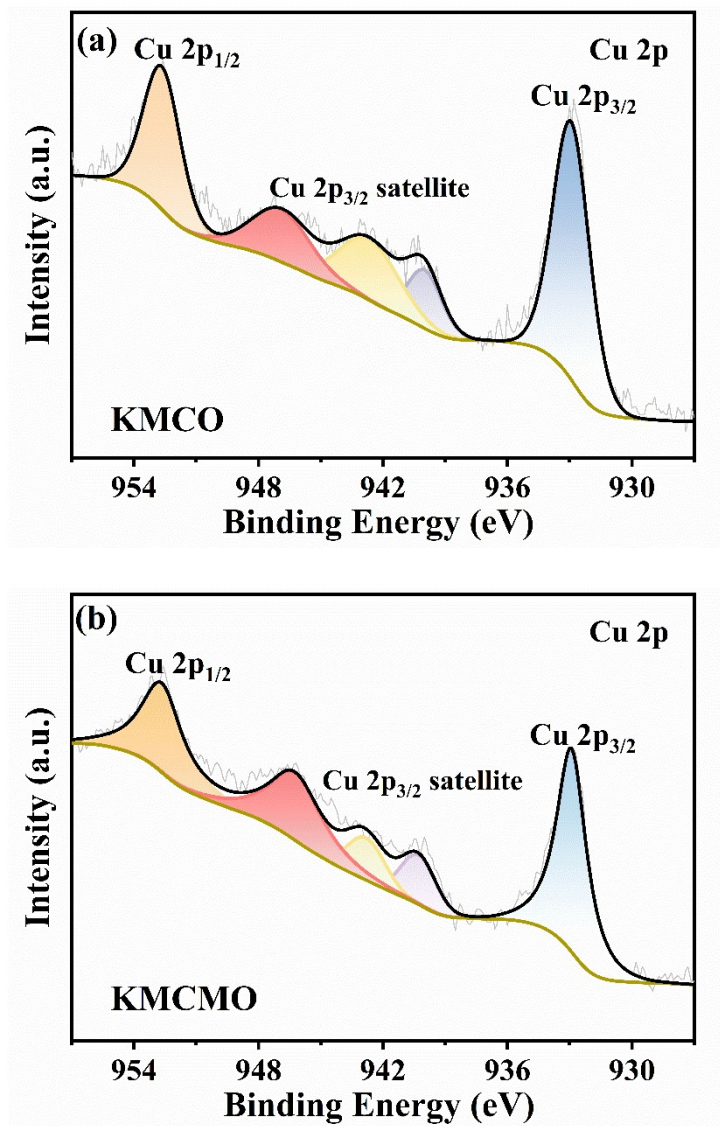**Figure S4**. XPS spectra of full spectrum of KMO and KMCMO samples.

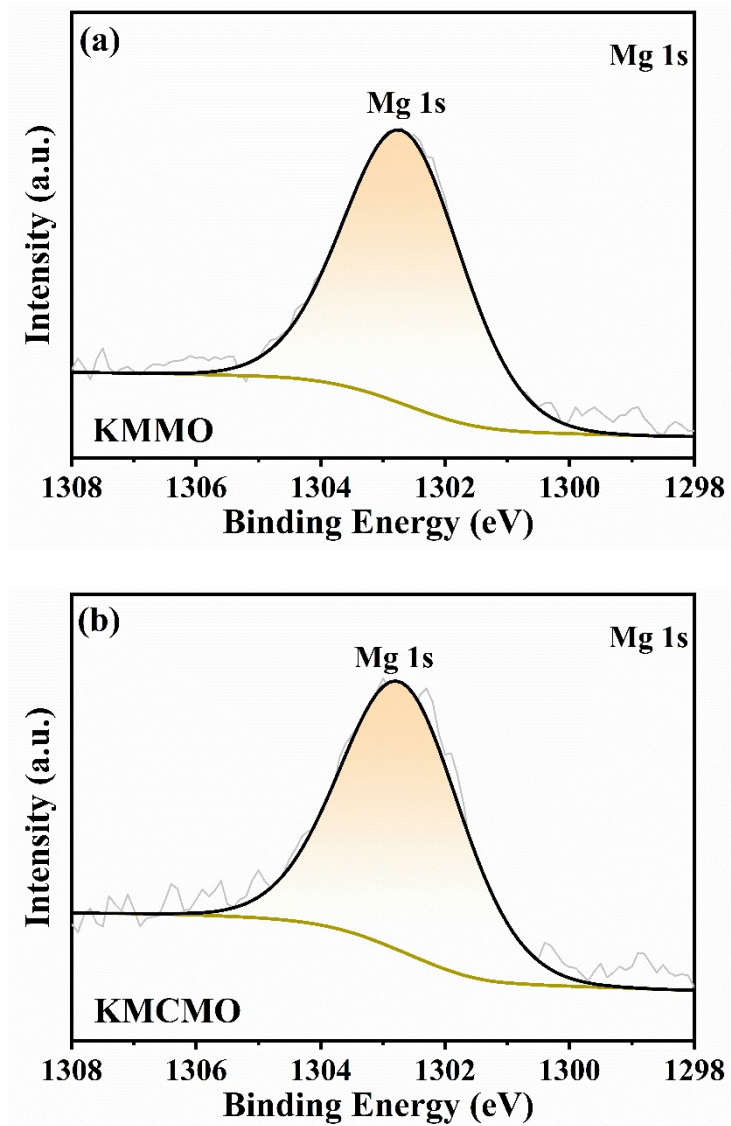**Figure S5**. XPS spectra of Cu 2p of KMCO and KMCMO samples.

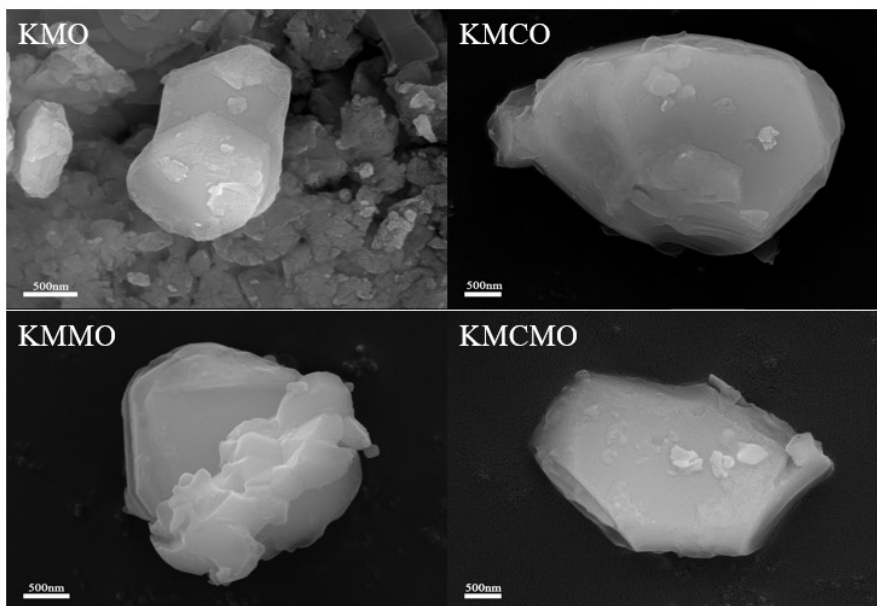**Figure S6**. XPS spectra of Mg 1s of KMMO and KMCMO samples.
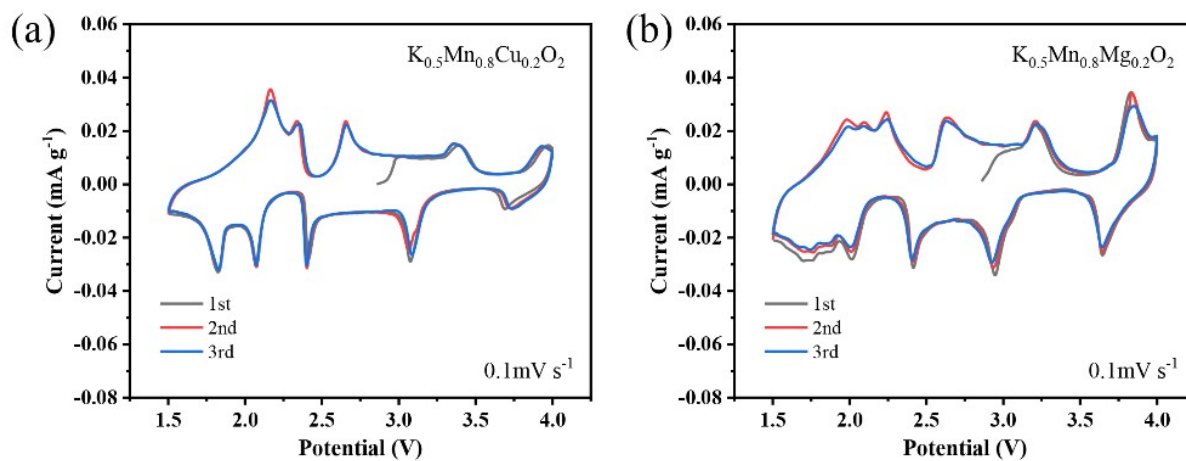
Figure S7. SEM of KMO, KMCO, KMMO and KMCMO samples.
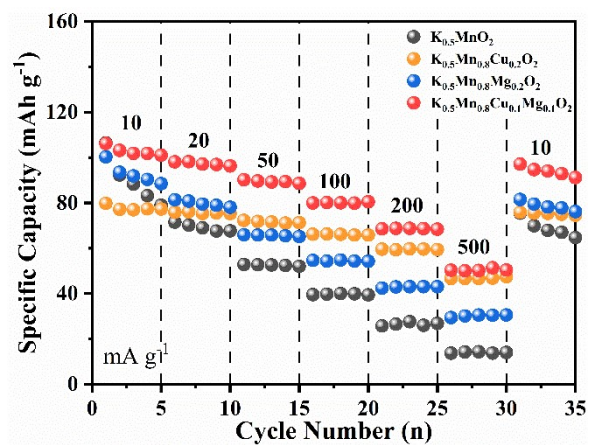

Figure S8. CV of KMMO and KMCMO samples.

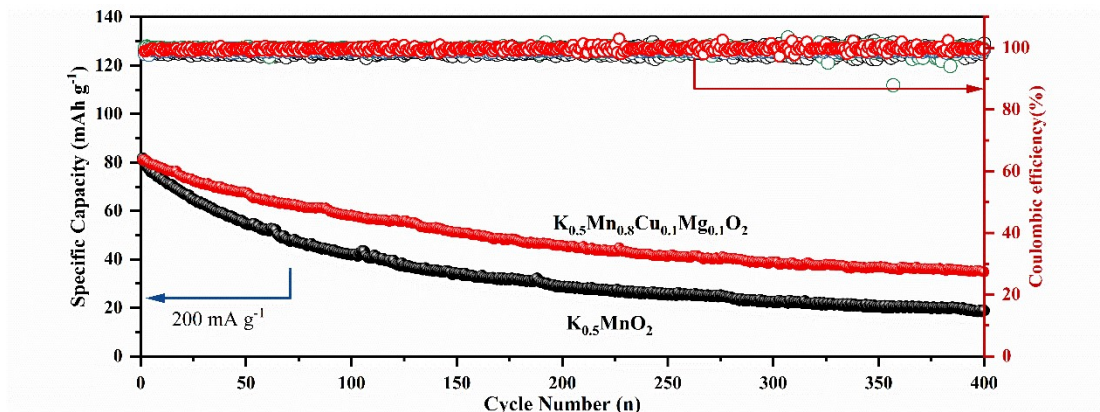**Figure S9.** Rate performances of KMO, KMCO, KMMO and KMCMO samples

Figure S10. Cycling performances of KMO and KMCMO samples.
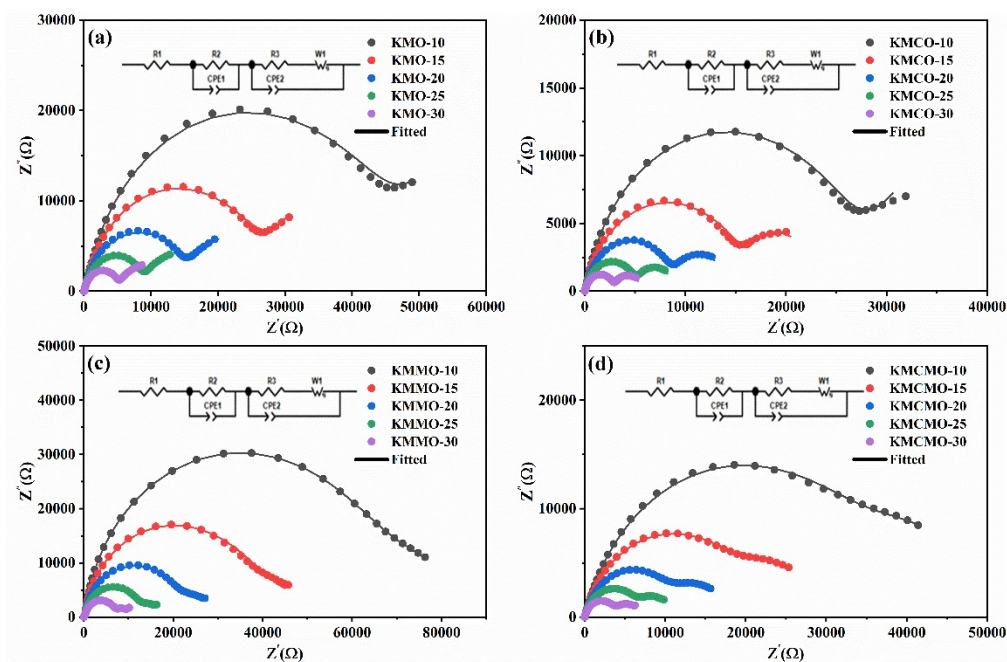

Figure S11. Nyquist plots of f KMO, KMCO, KMMO and KMCMO samples at different temperature.
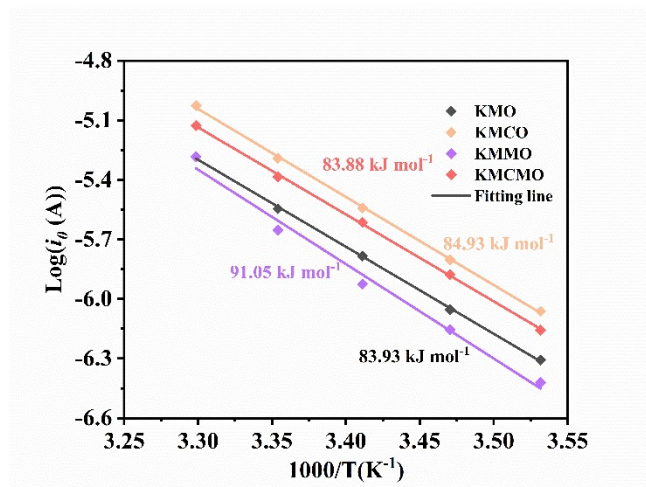

Figure S12. The fitting result of f KMO, KMCO, KMMO and KMCMO samples for Nyquist plots.

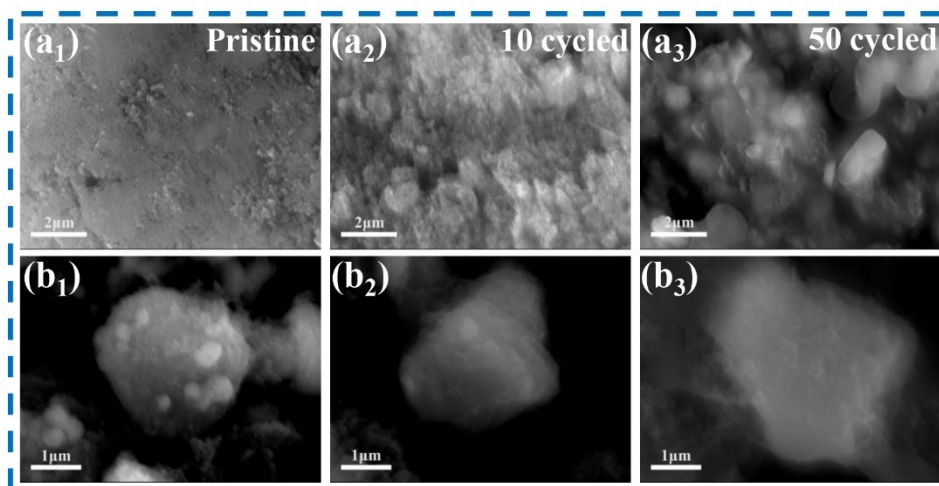**Figure S13.** Evolution of particle cracks. SEM images of the cross section of (a1-a3) KMO electrode and (b1-b3) KMCMO electrode at 200 mA g^{-1} after 0, 10, 50 cycles.
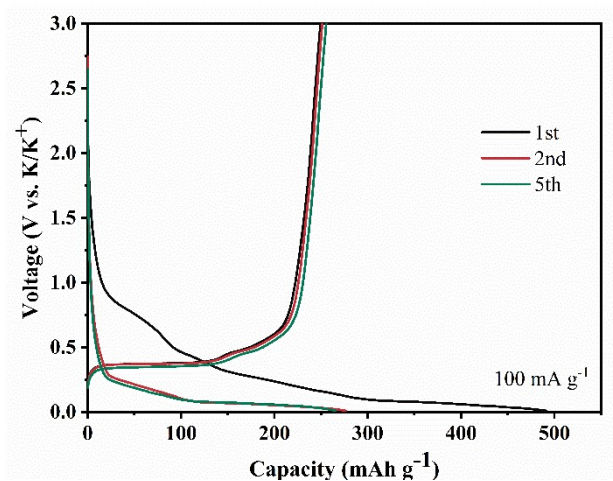

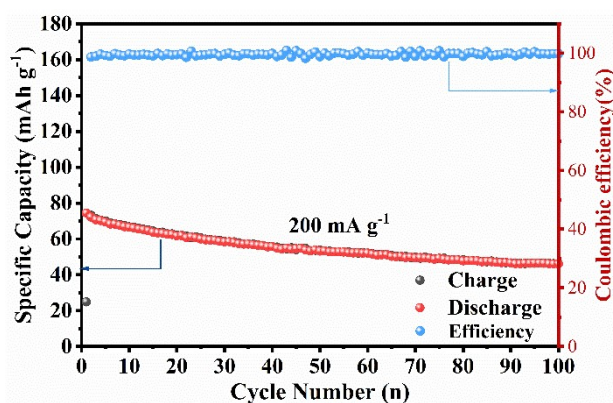**Figure S14.** Electrochemical performance of graphite in half-cell.

Figure S15. Electrochemical performance of KMO graphite in Full-cell at 200 mA g^{-1}.

Table S1. Structural parameters of KMO, KMCO, KMMO and KMCMO samples from Rietveld refinement.

Samples	a	b	c
$K_{0.5}MnO_2$	5.047	2.844	7.069
$K_{0.5}Mn_{0.8}Cu_{0.2}O_2$	5.046	2.862	7.090
$K_{0.5}Mn_{0.8}Mg_{0.2}O_2$	5.103	2.883	7.163
$K_{0.5}Mn_{0.8}Cu_{0.1}Mg_{0.1}O_2$	5.049	2.931	7.213

Table S2. Electrochemical data of some reported K half batteries containing layered oxide cathodes.

No.	Samples	Synthesis method	Current density (mA g^{-1})	Capacity (mAh g^{-1})	Refs.
1	P3-K0.67Ni0.17Co0.17Mn0.66O2	Co-precipitation and solid-state	20	77	[1]
2	$P2-K_{0.75}Mn_{0.8}Ni_{0.1}Fe_{0.1}O_2$	Electrochemical ion-exchange	100	80	[2]
3	P3/P2 $K_{0.37}Na_{0.3}Ni_{0.17}Co_{0.17}Mn_{0.66}O_2$	Co-precipitation and solid-state	20	86	[3]
4	$K_{0.45}Ni_{0.1}Fe_{0.1}Mn_{0.8}O_2$	Co-precipitation and solid-state	20	90	[4]
5	$Li_{0.27}K_{0.72}Ni_{0.6}Co_{0.2}Mn_{0.2}O_2$	electrochemical exchange	10	86.9	[5]
6	$K_{0.5}MnO_2$	solid-state	20	80	[6]
7	$K_{0.45}MnO_2$	Co-precipitation and solid-state	200	51.2	[7]
8	$K_{0.4}MnO_2 \cdot 0.36H_2O$	solid-state	80	90	[8]
9	K_xCrO_2	solid-state	150	80	[9]
10	$\mathbf{K_{0.5}Mn_{0.8}Cu_{0.1}Mg_{0.1}O_2}$	**sol-gel method**	**200**	**85.1**	**This**

References

1. C. L. Liu, S. H. Luo, H. B. Huang, Z. Y. Wang, A. M. Hao, Y. C. Zhai and Z. W. Wang, *Electrochem Commun*, 2017, **82**, 150-154.

2. J. Y. Hwang, J. Kim, T. Y. Yu, H. G. Jung, J. Kim, K. H. Kim and Y. K. Sun, *J. Mater. Chem. A*, 2019, **7**, 21362-21370.

3. C. L. Liu, S. H. Luo, H. B. Huang, Y. C. Zhai and Z. W. Wang, *Electrochim Acta*, 2018, **286**, 114-122.

4. R. B. Dang, Q. B. Yan, E. Y. Zhao, N. Li, K. Wu, Z. J. Chen, Z. H. Wu, X. F. Liu, Z. B. Hu and X. L. Xiao, *Sci. China Mater.*, 2022, **65**, 1741-1750.

5. W. Sohn, J. S. Chae, G. H. Lim and K. C. Roh, *J. Alloy Compd.*, 2022, **898** 162904.

6. H. Kim, D. H. Seo, J. C. Kim, S. H. Bo, L. Liu, T. Shi and G. Ceder, *Adv. Mater.*, 2017, **29** 1702480.

7. C. L. Liu, S. H. Luo, H. B. Huang, Y. C. Zhai and Z. W. Wang, *Chem. Eng. J.*, 2019, **356**, 53-59.

8. A. Gao, M. Li, N. N. Guo, D. P. Qiu, Y. Li, S. H. Wang, X. Lu, F. Wang and R. Yang, *Adv. Energy Mater.*, 2019, **9** 1802739.

9. W. Ko, J. Kim, J. Kang, H. Park, Y. Lee, J. Ahn, B. Ku, M. Choi, H. Ahn, G. Oh, J.-Y. Hwang and J. Kim, *Mater. Today Energy*, 2023, **36** 101356.